Available online at www.sciencedirect.com
ScienceDirect
Ceramics International 35 (2009) 1731–1746
CERAMICS INTERNATIONAL
www.elsevier.com/locate/ceramint

Crack formation, exfoliation, and ridge formation in 500 °C annealed sol–gel silica coatings on stainless steel SUS304: Part I. Microscopic observations and elemental analyses

Makoto Takemori *

Research Institute for Environmental Management Technology, National Institute of Advanced Industrial Science and Technology (AIST), 16-1, Onogawa, Tsukuba 305-8569, Japan

Received 5 May 2008; received in revised form 3 June 2008; accepted 30 September 2008
Available online 5 November 2008

Abstract

Uniformly compact silica coatings of thicknesses >400 nm on Cr- and Ni-containing steels are practically desirable but difficult to obtain. A non-aqueous sol–gel silica coating on SUS304 was studied. After the coated substrates were treated at 500 °C in air, coatings with thicknesses of ~350 to ~1000 nm were obtained that were largely uniform, non-porous, adherent, and with minimal residual organic content, although some cracks and exfoliated sites existed. TEM/EDX analysis indicated that three interlayers were observed between silica and SUS. The innermost one was ~5 nm thick, Cr-rich, highly O-deficient, and formed a tenacious bond between SUS304 and silica; the two others were rather diffuse. The web-like development of ridges resulting from the oxidation of metallic elements (mostly Fe) diffused into the silica through nanoscale defects within the innermost interlayer was also observed. Many of the nanoscale defects seem to be related to SUS grain boundaries. Ni was almost absent in silica coating except in the innermost interlayer and ridges. The mechanisms responsible for these observed properties and phenomena are discussed.

Keywords: A. Films; A. Sol–gel processes; B. Interfaces; D. SiO_2

1. Introduction

Silica-based, compact adherent coatings that are used to coat the surfaces of Cr- and Ni-containing steels, especially stainless steels such as SUS304, are useful for many practical applications. (The term 'SUS' refers to the Japanese standard of stainless steel and the same as 'AISI', but in this report the term is also used to refer to stainless steel in general.) For example, these coatings are used as Cr^{6+}-free corrosion-resistant coatings [1–5], as coatings on discharge electrodes for environmental applications [6], as wear resistant coatings [7], as electrical insulating coatings [8], and as barrier coatings against nitridation of SUS [9]. For these applications, coatings with thickness >400 nm are favorable. These coatings should be of 'good quality,' that is, compact, uniform, adherent, sufficiently hard, smooth, without excessive organic or moisture content, and desirably transparent. Additionally, when SUS304 substrates are to be coated, the heat treatment temperature should not exceed ~600 °C, so that severe sensitization is prevented [10].

Several methods for the preparation of silica-based coatings have been reported, and some are already in practical use. Some kinds of chemical vapor deposition (CVD) methods [4], including plasma-enhanced CVD [11] and laser-induced CVD [12], produce good-quality silica coatings. However, such methods usually require special equipment, and moreover, the use of these methods for coating products that are large, complex in shape, or both is difficult. Electrophoretic coating is a promising alternative method for the fabrication of silica-based thick coatings, but the produced films tend to be porous [13], and other problems are associated with the use of electrodes in this method, *e.g.* H_2 bubbling [14] and electrode elusion [15]. Reports on 'good quality' silica coatings prepared on SUS by non-electrophoretic methods using extra powders are rare.

Possible alternatives to CVD and electrophoretic methods are chemical solution methods without extra powder addition. They are categorized into two major groups: liquid-phase

* Tel.: +81 29 861 8180; fax: +81 29 861 8459.
E-mail address: takemori.mkt@aist.go.jp.

0272-8842/$34.00
doi:10.1016/j.ceramint.2008.09.014

deposition (so-called LPD) methods [16] and non-electrophoretic sol–gel methods [1–3]. LPD methods are advantageous because they do not require heating, but are problematic because they require toxic H_2SiF_6 aqueous solutions. Furthermore, LPD methods cannot be easily applied to substrates such as SUS because of usually corrosive nature of SUS in H_2SiF_6 solutions [16].

By contrast, non-electrophoretic sol–gel methods require neither special equipment nor highly toxic reagents, and moreover, are potentially applicable to products that are large, complex in shape, or both. Vasconcelos et al. [2] treated AISI304 substrates with an aqueous sol–gel coating liquid and heated them to 600 °C. They acquired crack-free silica coatings of ≤120 nm thickness with fairly good, but not ample corrosion resistance. Traditionally, sol–gel silica coating methods that utilize neither an electrode, nor the addition of extra powders, nor special reagents (*e.g.* reagents containing Si–C [15] or Si–N bonds [17]), nor irradiation of light [18] rarely yield coatings of good quality with thicknesses greater than 400 nm obtained in a single coating cycle [19]. (Thick coatings of borosilicate [20] and aluminosilicate [21] prepared by sol–gel methods have been reported, however.) Sol–gel silica coatings with thicknesses of several μm have been deposited on various substrates through the incorporation of large amounts of Si–C containing species such as methyltriethoxysilane, but many Si–C bonds are undesirable because they often increase O-permeation [22] and softness [23]. It is true such bonds are reported to promote adherence [24], but not above ∼500 °C [23]. Methods utilizing reagents containing Si–N bonds (*i.e.* silazanes) are effective [17], but these reagents are often highly reactive and besides inflammable, a little toxic and expensive; furthermore, coatings substantially thicker than 1 μm that are obtained from a single coating cycle are rarely reported. Although not exactly a 'sol–gel' method, SUS304 has been coated with melt silica glass powders at temperatures low as ∼500 °C [25]; however, metallic elements within SUS are oxidized, thus deteriorating the coating mechanically and chemically.

The present report (Part I), together with the following one (Part II), describes the fabrication of substantially thick (∼1 μm) sol–gel silica coatings that exhibit 'good quality' on alloys such as SUS304 under the conditions described above (*i.e.* non-electrophoretic sol–gel, without special equipment, without reactive and/or toxic reagents, without extra powder, treatment as low as ∼600 °C). The sol–gel silica coatings were prepared by a previously reported non-aqueous method [26] on SUS304, and 'good-quality' coatings were partially attained. In Part I, results of microscopic observations and elemental analyses are described, and these results are interpreted in terms of film formation processes.

2. Experimental procedures

2.1. Sol–gel coating

Bright annealed SUS304 plates of the atomic and weight percent composition shown in Table 1 were used as substrates. The elements reported in Table 1 were chosen for quantitative chemical analysis by conducting a qualitative X-ray fluorescence screening on the substrates.

Silica-coated substrates were prepared in triplicate and are referred to as Samples 1–3 hereafter. The substrates were coated with silica according to the non-aqueous sol–gel method reported previously [26]. Briefly, 20-ml portions of tetraethylorthosilicate (TEOS) and acetic acid were mixed and then heated at ∼120 °C for ∼60 min; then, 20 ml *n*-hexane was added and the mixture was again heated at ∼120 °C for ∼60 min; finally, a second 20-ml portion of *n*-hexane was added and the mixture was heated at ∼120 °C for ∼450 min. The SUS304 plates were dipped in the resulting solution, and the dip-coated substrates were heated in air atmosphere from room temperature to 150 °C (temperature not programmed exactly but reached in ∼26 min and kept for ∼94 min). The temperature then was raised to 190 °C (reached in ∼15 min and kept for ∼825 min) before the plates were cooled in the furnace, soaked in water for about 5 h, heated again at 190 °C (reached in ∼37 min and kept for ∼803 min), and cooled again in the furnace. This process is referred to herein as the 'first heating process.' The samples were then heated in air from room temperature to 500 °C at 5.5 °C min^{-1}, kept at 500 °C for 120 min, and then cooled in the furnace. This process is referred to herein as the 'second heating process.'

For Samples 1 and 2, SUS plates of 50 mm × 50 mm × 1 mm-thick dimensions were used immediately after removal of their protective polymer films and washing with ethanol. The samples were vertically suspended during the dip-coating and the first heating process, and then placed horizontally in the furnace for the second heating process. (The withdrawal rate of dip-coating was ∼10 mm/s. The dip-coated parts were ∼15 mm from the lower edge, and the upper parts remained uncoated, but these parts were treated without separation afterward in the coating treatments.) In contrast, Sample 3 utilized a 2.5 mm × 2.5 mm × 1 mm-thick SUS plate, mechanically cut from a large SUS plate, but the dip-coating process was modified as follows: a small amount of the silica coating solution was dropped onto the substrate, which was placed on a glass plate. The glass plate was then tilted to allow the excess coating liquid to flow over the substrate before the plate was laid flat again. Following this coating procedure, Sample 3 was heated during *in situ* OM observations as described in the following section.

Table 1
Composition of the SUS304 samples.

	C	Co	Cr	Cu	Fe	Mn	Mo	N	Ni	O	P	S	Si
wt.%	0.055	0.22	18.02	0.24	Bal (71.5)	0.78	0.14	0.028	8.46	0.0052	0.033	0.006	0.53
at.%	0.25	0.2	19.01	0.21	(70.3)	0.78	0.08	0.11	7.9	0.018	0.058	0.010	1.0

'Bal' refers to remaining elements in the balance of the sample.

2.2. Characterization

Scanning electron microscopy (SEM), transmission electron microscopy (TEM) with energy dispersive X-ray spectroscopy (EDX), optical microscopy (OM), and laser microscopy (LM) were performed on the as-prepared samples. Specifically, Sample 1 was used for SEM and TEM/EDX analyses. The sample was cut with a focused ion beam (FIB) to provide pieces for these analyses. For OM analysis, Sample 2 was mechanically cut into appropriately sized pieces with a dicing saw using water. An additional piece of Sample 2 was cut with an FIB for TEM/EDX analysis. Sample 3 was, after the OM and LM observations, cut with an FIB along a line (indicated in Fig. 5(i) by a thin long yellow box), and the exposed cross-section was analyzed by TEM.

For SEM analysis, a scanning electron microscope (S-4500; Hitachi Ltd.) was used. For TEM/EDX analyses, a field emission transmission electron microscope (HF-2000; Hitachi Ltd.) equipped with an energy dispersive X-ray spectrometer was used. Samples for TEM/EDX analyses were, before FIB cutting, coated by carbon and heavy metal for protection.

An optical microscope (VHX-500; Keyence Ltd.) equipped with a conduction heating stage was used for OM measurements. Sample 2 was observed *ex situ* after cutting by a dicing saw using water. Sample 3 was observed *in situ* during heating in air from room temperature to 610 °C (set value) by means of the temperature program shown in Fig. 1. The temperature control was not completely accurate but appeared to be rather sufficient, judging from the resulting OM images. For example, at a set temperature of 500 °C, the observed temperature was 450–550 °C. (Measurement of the actual temperature of Sample 3 was difficult, because a thermometer was not attached directly to the sample for fear of contamination.) Following the *in situ* annealing process during OM observations, Sample 3 was observed by LM with a laser microscope (VK-9500; Keyence Ltd.). Both a two-dimensional (2D) and a three-dimensional (3D) image of the outer surface were obtained.

3. Results

3.1. Physical appearance of the samples

The silica-coated substrates that were obtained after the dip-coating and the first heating process exhibited largely uniform silica films, with neither cracks nor exfoliation present apparently. These samples appeared only slightly more yellow than the as-received glossy SUS304 plates, but the silica film was not stiff and could easily be scraped off with a stainless steel spatula. For Samples 1 and 2, coating was already lost in the lower region, *i.e.* ∼5 mm from the lower edges of the upright SUS304 plates, where overly thick liquid films were formed after the dip-coating but exfoliated already after the 190 °C annealing of the first heating process.

Following the second heating process of Samples 1 and 2, larger silica-coated areas remained without exfoliation, but these films could not be scratched off manually with a stainless steel spatula. These samples appeared grayish yellow and slightly hazy.

3.2. OM and LM results

As shown in Figs. 2 and 3, cracks were initiated at some points and propagated during high-temperature annealing of Sample 3. The coating surface around the initiation point of the large extended parabola-shaped crack that was observed by OM (Fig. 2) was further analyzed by LM. The silica coatings were not substantially exfoliated and retained good transparency both during and after the high-temperature annealing process, *i.e.* the silica/SUS304 interface was observed through the non-exfoliated silica coating by OM. Small exfoliated areas were observed for Sample 2, on the contrary, but the coating's transparency was also good. Both colored features near the SUS plate and shallow cracks near the silica surface were observed by adjusting the distance between the sample and the OM objective lenses (Fig. 4). A flaky transparent exfoliated film and black dust particles were observed after cutting, but were removed by gentle wiping with degreased cotton immersed with tetrahydrofuran. Darkly colored

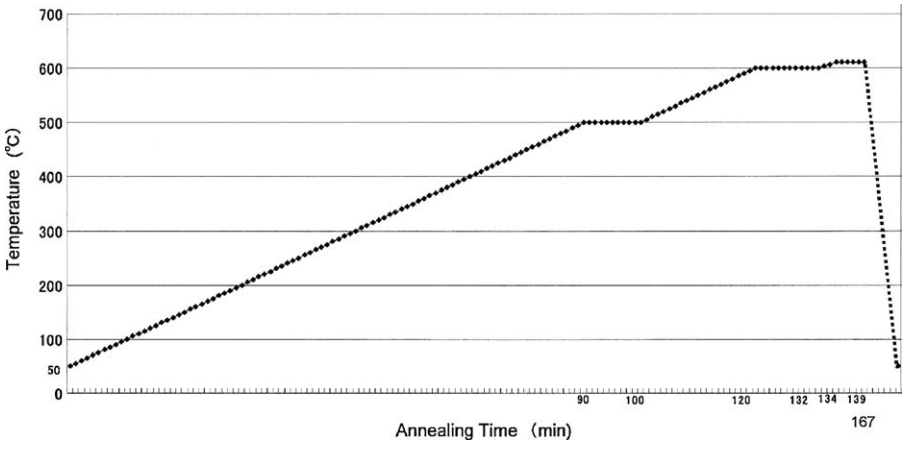

Fig. 1. Temperature program for *in situ* heating of Sample 3 during OM analysis.

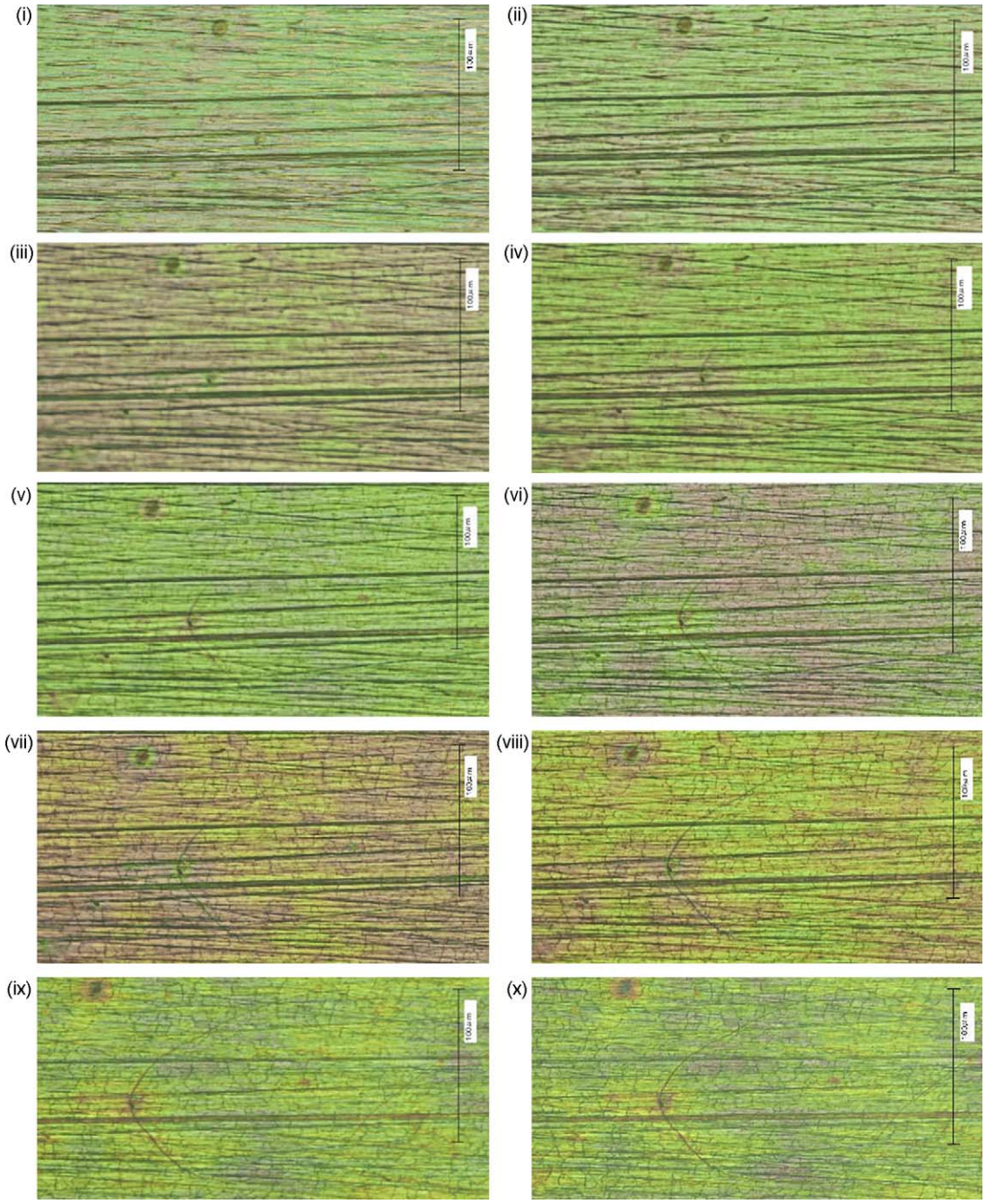

Fig. 2. Typical OM images of Sample 3 acquired during *in situ* heat treatment at (i) 1 min, (ii) 63 min, (iii) 71 min, (iv) 74 min, (v) 78 min, (vi) 82 min, (vii) 88 min, (viii) 93 min, (ix) 117 min, and (x) 149 min.

irregularities of ∼100 nm width spanning large areas of the samples were observed by OM focused at the silica/SUS304 interface (seen especially clearly in Figs. 4(i) and 5(iii)). These irregularities are referred to as 'ridges' hereafter. Most of the ridges were web-like, and some had developed along scratches already present on the as-received SUS304 surface. However, many isolated dark ridges were present as well. (Interestingly, similarly shaped structures were reported for a silica coating prepared by thermal decomposition of TEOS at 750–800 °C on strongly passivated AISI316L substrates, but those ridges were much bigger [8].)

Numerous deep and shallow cracks were observed on the samples. These cracks were typically running almost irrespective of pre-existing scratches on SUS304. Some of the shallow cracks appeared trench-like in structure (*ex situ* Fig. 5(ii)). The deep cracks appeared to have evolved after the formation of the ridges and were mostly straight in lateral directions, but sometimes curved, branched, or both. The crack branches were usually T-shaped rather than Y-shaped. Some of the deep cracks were initiated at irregular points, *e.g.* at points where accidentally incorporated inclusion particles existed; but most of these cracks did not have clearly defined initiation points.

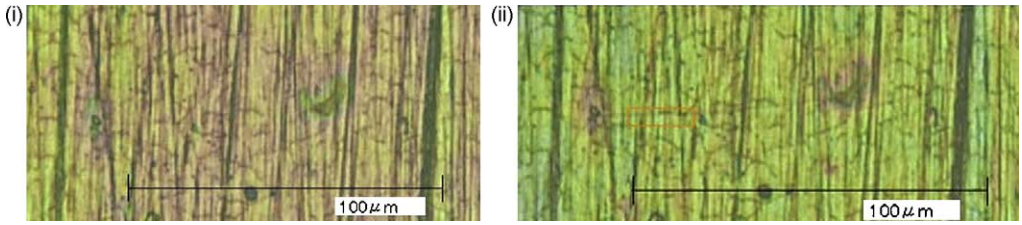

Fig. 3. Atypical OM images of Sample 3 acquired during *in situ* heat treatment at (i) 86 min and (ii) 92 min. A deep crack running along a ridge is shown in the orange box in (ii). (For interpretation of the references to color in this figure legend, the reader is referred to the web version of the article.)

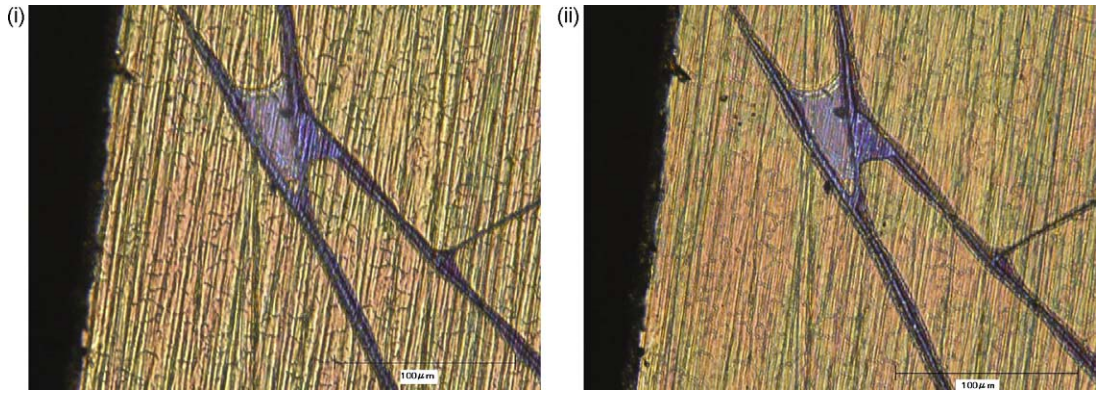

Fig. 4. OM images of Sample 2 (i) focused near the silica coating/SUS304 interface and (ii) focused near the outermost surface of silica coating. The left side of this sample was cut with a dicing saw (see also text).

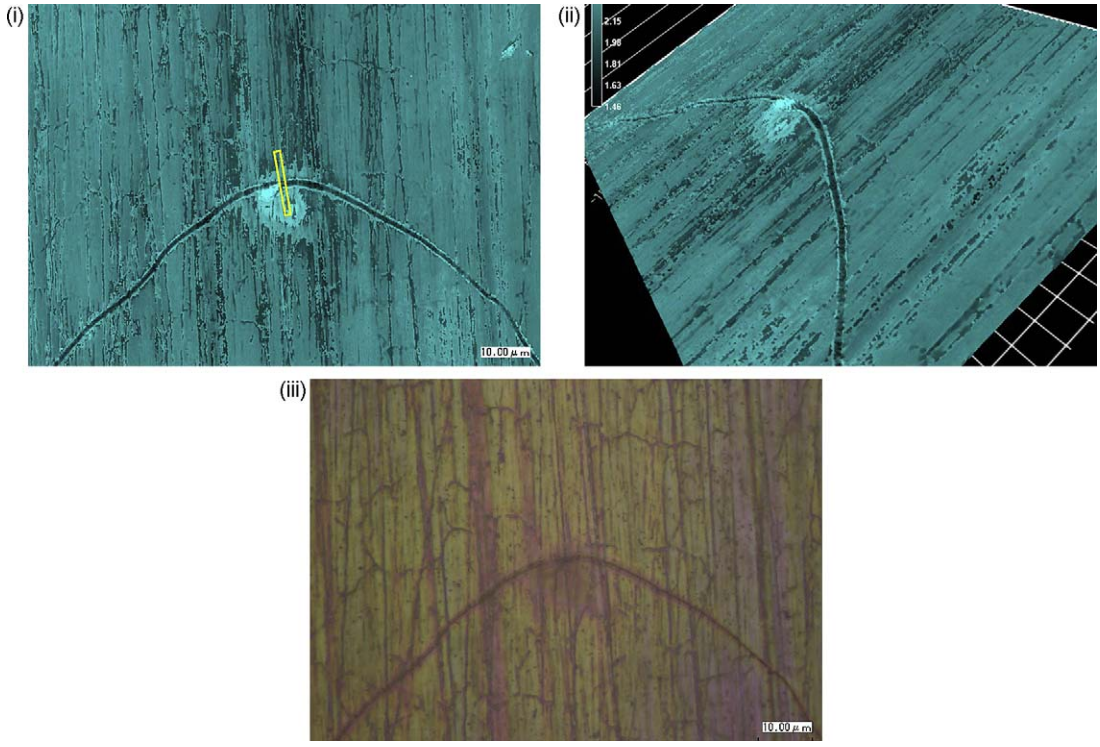

Fig. 5. LM and OM images of Sample 3 showing the initiation point of a parabola-like crack: (i) LM-2D image, (ii) LM-3D image, and (iii) OM image. The thin long yellow box shows the FIB cutting line. (For interpretation of the references to color in this figure legend, the reader is referred to the web version of the article.)

Examples of deep and long extending crack developments are shown consecutively in Fig. 2(i)–(x). A clear irregularity in the silica coating (probably an inclusion particle in the coating) that served as an initiation point for the parabola-shaped large crack was observed *in situ*. Comparison of Fig. 5(ii) with Fig. 5(i) and (iii) reveals that some of the trench-like shallow cracks were accompanied by ridges. A deep crack propagating along a ridge was also observed *in situ* (Fig. 3; observed most apparently in

the orange box in Fig. 3(ii)). The location of this crack was an exception to the general location of the deep cracks observed in these samples, as the deep cracks generally did not follow the ridges or mechanical scratches on the SUS304 substrate. By contrast, as described just above, some shallow cracks did form along the ridges.

Exfoliation was observed for Samples 1 and 2 after they were cooled from high temperature, but exfoliation was not observed for Sample 3, whose period of high-temperature treatment was much shorter. The portions of SUS304 substrate in Samples 1 and 2 that were exposed owing to exfoliation were dark blue or dark russet, as shown in Fig. 4(i). The tint was similar to that of an uncoated area of SUS304 surface after heating to 500 °C in air.

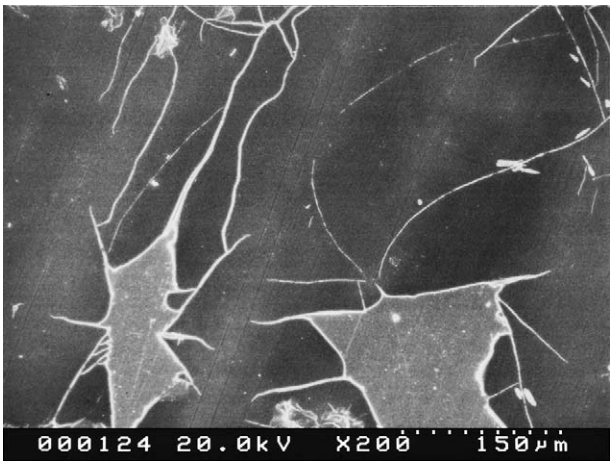

Fig. 6. SEM image of Sample 1, showing exfoliation of the silica coating (light regions). Unexfoliated portions of the sample are fairly flat, but pre-existing scratches on the SUS304 are also visible.

3.3. SEM and TEM/EDX results

The sample surfaces were generally uniform, but some parts showed cracks and exfoliation, as seen in the SEM image (Fig. 6). The unexfoliated parts of the samples were fairly flat, although some pre-existing scratches that were present on the SUS304 substrate before coating could be traced on the outermost surface after coating. Figs. 7 and 8 show cross-sectional TEM images of the samples. Labels 'A', 'B', 'B′', 'C', 'D', and 'E' in Fig. 7(iii) and (iv) correspond to he silica matrix, the third interlayer, a ridge, the second interlayer, the innermost interlayer and the SUS304 substrate, respectively. A coating thickness of ∼550 nm was observed for Sample 1. Thinner (∼350 nm) and thicker (∼1 μm, data not shown here) portions were seen on Sample 2. A thicker (∼1 μm) portion was observed also for Sample 3. But the features near the silica/SUS304 interface were basically the same for all three samples. There was no clear relationship between film thickness and crack formation.

The silica matrix was microscopically compact and uniform, appreciably more so than that usually reported for sol–gel silica

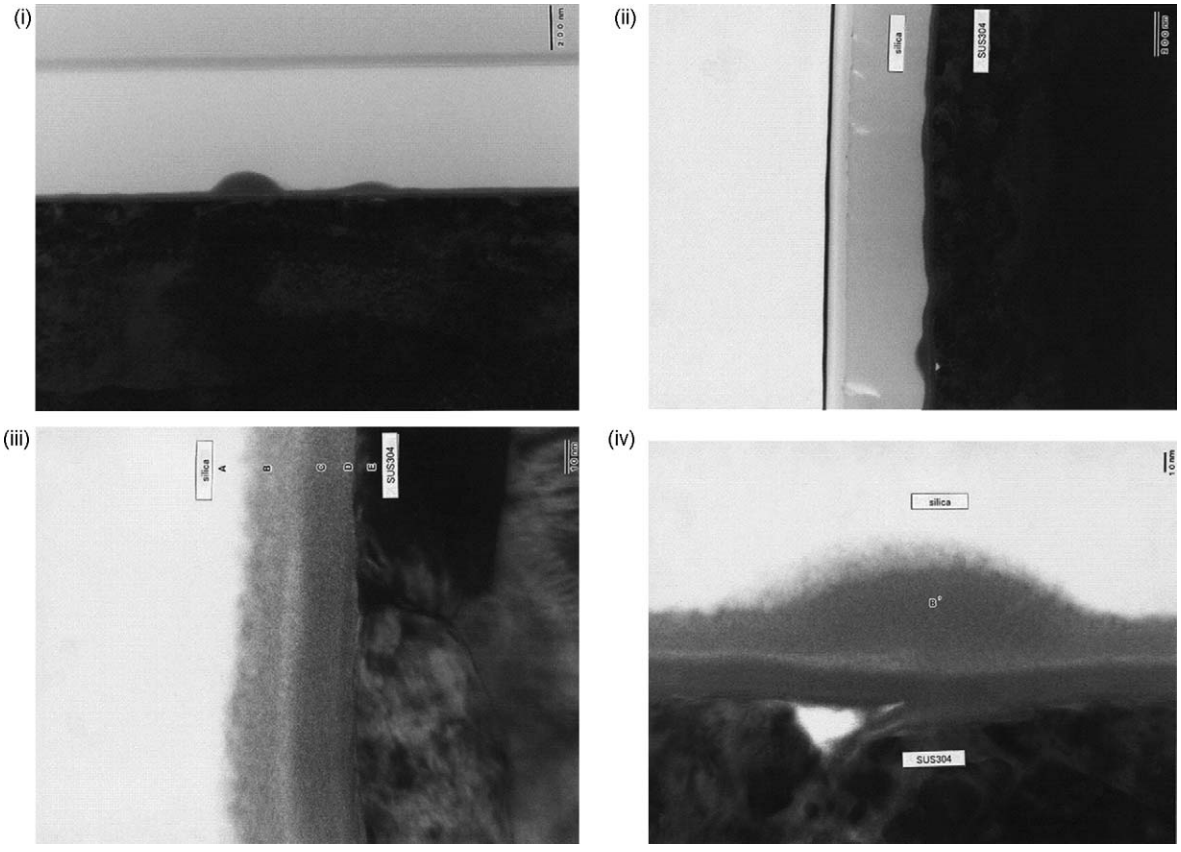

Fig. 7. Cross-sectional TEM images: (i) Sample 1; (ii), (iii) and (iv) Sample 2. The labels in these images are defined in the text.

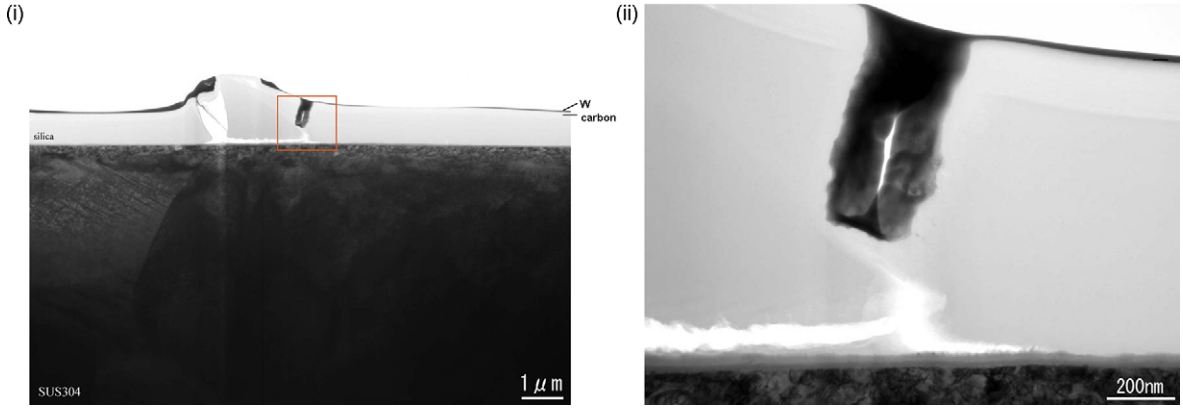

Fig. 8. Cross-sectional TEM images of Sample 3 with (i) lower magnification and (ii) higher magnification of the orange box of (i). (For interpretation of the references to color in this figure legend, the reader is referred to the web version of the article.)

after ∼500 °C annealing [27,28]. Three consecutive interlayers existed between the silica and SUS304 substrate, and there were very few micro-cracks and voids in these regions (see Part II). Within the seemingly adherent parts of the coating, ridges of ∼100 nm width were often observed in the silica matrix by TEM as well as by OM, but these ridges were not observable by SEM when looking at the outermost surface of the silica coating. Ridges were often present at the places where grain boundaries of the SUS304 substrate met with the interface; however, grain boundaries without accompanying ridges were also present. Some of the ridges were adjacent to voids in the SUS304 substrate, to cracks from the outermost silica surface, or to both. Such distinct voids were absent in the deeper (>∼50 nm) parts of the SUS304 substrate. Cracks and exfoliations, were mostly unrelated to the pre-existing scratches, however scratches were often accompanied by ridges.

Table 2 shows the EDX results obtained around the interlayers and at a ridge. Each label ('A', 'B', 'B′', 'C', 'D', or 'E') in the far left column of the table corresponds to the location with the same label in TEM images of Fig. 7(iii) and (iv). The innermost interlayer was thin (∼5 nm) and distinct, containing metallic elements in the following order of EDX intensity: Cr > Fe ≫ Si > Ni. This layer was highly O-deficient (see also Section 4.1.2). However, the Ni content was appreciably higher in the innermost interlayer than in other parts of the coating. Two comparatively thick diffuse interlayers were also present, and both of these layers were O-deficient to some extent. The middle interlayer exhibited EDX intensities that decreased in the order Cr ≫ Si ≫ Fe ≫ Ni, and the outermost interlayer exhibited EDX intensities that decreased in the order Si > Fe ≫ Cr (Ni was not detected in this case). The two diffuse interlayers were separated by a short distance of several nm. EDX data collected at the ridge indicated that the ridge area was slightly O-deficient with metallic element intensities that decreased in the order Fe > Si ≫ Ni ≒ Cr. TEM/EDX results of the interlayers for Sample 1 were qualitatively the same as those for Sample 2, but the innermost layer of Sample 1 was slightly more abundant in Fe content (data not shown).

Table 2
EDX results of the microscopic parts shown in Fig. 7(iii) and (iv).

	Si (at.%)	Fe (at.%)	Cr (at.%)	Ni (at.%)	O (at.%)
A	39.5	0.3	0.1	0.0	60.1
B	29.2	13.1	0.2	0.0	57.5
B′	16.4	31.1	0.2	0.3	52.0
C	7.4	1.7	37.6	0.1	53.2
D	3.9	10.2	39.1	1.9	44.9
E	0.3	69.6	17.2	7.7	5.2

The labels used in the far left column are defined in the text.

As shown in Fig. 7(ii), cracks from the outermost surface of silica, but without approaching SUS304, were rather vertical and their tips were rather dull. Most of these cracks were shallow, although an intermediately deep crack was present near a ridge. Cross-sectional TEM images of Sample 3 are shown in Fig. 8 with lower (i) and higher (ii) magnifications. Before the TEM observations, the sample was cut with an FIB after OM and LM observations, so as to define the cross-section in the area denoted by the thin long yellow box in Fig. 5(i). The inclusion particle visible in Fig. 5 must have existed during the 500 °C annealing process, causing the crack initiation described above; however, this particle was somehow removed from the sample prior to TEM measurements, as it is not visible in Fig. 8, and a vacant space is instead visible in its place. Fig. 8(ii) clearly shows that the lateral cracks propagated for some distance along the edge of the outermost diffuse interlayer.

4. Discussion

4.1. Crack evolution and exfoliation of compact silica coating

The reason for the relative compactness of the present silica films as compared to films reported in the literature [27] is fairly unclear. However, in the present process notably, water was not added intentionally to the sample until the end of the first 190 °C annealing step in the first heating process. Quite possibly, micro-pore formation within the samples was minimal because most of the water, the amount of which could not have

been so much, had evaporated before the temperature of the samples reached ∼500 °C.

The reason for the differences between the thicknesses of the three samples was not clear. Vasconcelos et al. have reported that the thicknesses of their sol–gel-prepared silica coatings are not well-reproduced [2]. The observed variations in film thicknesses might be attributed to differences in the degree of Si–O–Si bond development in the coating liquid: sol–gel silica coating films have been reported to thicken as their precursor liquids age [28]. Other factors, such as differences in the sizes of SUS304 substrates, might have influenced the variations in thickness as well.

Although a large portion of the silica coating was adhered to the SUS304 substrate after the ∼500 °C treatment, both deep and shallow cracks as well as exfoliation were observed by OM (Figs. 2–4), LM (Fig. 5), SEM (Fig. 6), and TEM (Fig. 7(ii) and Fig. 8). The evolution of deep cracks during high-temperature annealing was observed *in situ* by OM (Figs. 2 and 3), but exfoliation was not directly observed. Nevertheless, exfoliation most likely occurred during the high-temperature annealing rather than during or after cooling, contrary to the so-called spallation reported with cyclic oxidation [29], because the tint of the exfoliated regions of the sample (Fig. 4) following prolonged high-temperature annealing resembled that of the uncoated part of the SUS304 surface.

The shallow cracks also most likely were formed and terminated in the early stages of the high-temperature annealing process, because their dulled tip shapes (Fig. 7(ii)) indicate that their propagations were terminated before the silica matrix became substantially rigid. However, some shallow cracks may have continued to propagate, evolving into deep cracks that might have subsequently promoted exfoliation. Both the shallow cracks and the deeper ones whose propagation terminated without any clear diversion to the lateral direction are herein referred to as 'vertical crack(s),' although they were not always strictly vertical.

4.1.1. Initiation and propagation of vertical cracks

The formation of cracks during the drying and annealing of sol–gel silica-based coatings is typical [30]; nevertheless, the cause and evolution of these crack formations should be discussed in the context of the present results. From *in situ* OM observations at high temperatures, it is naturally inferred that the elimination of organics (through evaporation, oxidative decomposition, or both) and of a little amount of water (humidity) should have led to shrinkage of the coating, which in turn resulted in lateral tension (see Part II), causing cracks to form. Both humidity and organics were most likely absent from the samples at least in the later stages of the 500 °C annealing process of Samples 1 and 2 (see also FT-IR results and interpretation in Part II). However, the microscopically compact nature of the present silica matrix as compared to matrices of ∼500 °C treated sol–gel silica in the literature suggests that the present silica coatings' crack evolution should have been rather different from that of reported sol–gel silica coatings.

One possible mechanism of crack formation that is often mentioned in the literature is capillary force, *i.e.* the surface tension induced by water in the micro-pores of the silica matrix [31]. However, experimental conditions and observations indicate that capillary force was not a major cause of crack formation in the present samples. For example, water was not added intentionally to the coating liquid. The samples were soaked in water during the first heating process but were subjected to prolonged annealing at 190 °C prior to annealing at 500 °C, and cracks were not observed after annealing at 190 °C. Additionally, the silica coating was observed to be almost microscopically non-porous after annealing of Samples 2 and 3 at 500 °C, indicating that the coating was probably minimally porous prior to and during the high-temperature (∼500 °C) annealing. Even if some water and pores were present prior to and during the 500 °C annealing, capillary force is generally not expected to occur at higher temperatures [32]. For these reasons, the observed crack formation in the present study must have been caused by another phenomenon.

The tension and cracks observed on the samples more likely resulted directly from the elimination of organics and water (humidity). More specifically, the tension produced by shrinkage probably was less diffused than is often reported for sol–gel coatings because the volume space of micro-pores, which act as deformation buffers by collapsing themselves, was small. Additionally, 'shrinkage-induced' tension might have been strengthened near the outer surface by the persistent adherence of the coating to the substrate. Incidentally, both shrinkage and increasing rigidity of the matrix during annealing are generally observed for sol–gel silica [33], and 'shrinkage-induced' cracks are somewhat typical among sol–gel coatings in general, as long as the coatings remain adherent. In other words, 'shrinkage-induced' cracks are expected given the adherent, almost non-porous nature of the present coatings. (Notably, on the contrary, silazane [17] and hydrogen silsesquioxane [34] are expected to eliminate volume shrinkage, and most probably the occurrence of cracks, in sol–gel silica coatings.)

The mechanism and location of crack initiation, as well as the mechanism of crack propagation, are also of interest. The experimental observations again provided insight into these mechanisms. From Fig. 7(ii), it is apparent that some cracks were initiated at the outer surface of the silica coating but did not propagate through the coating to the SUS304 substrate. Therefore, crack propagation appears to have occurred mainly through a 'top-down' rather than a 'bottom-up' mechanism.

I believe that the vertical cracks must have propagated mostly in a top-down process, rather than a bottom-up one, for two reasons. First, any remaining organics and humidity in the silica matrix must have escaped during the 500 °C annealing process, and some of the organics were probably burned off [26]. The escape rates of these materials must have been faster at the outermost surface than near the coating's interface with the substrate. Previously published SEM images [30] have shown instances in which a sol–gel SiO_2–TeO_2 coating shrank more at its outer surface than at its interface with a substrate, and recently I also observed a similar phenomenon with

adherent thick silica coatings prepared on a beaker glass substrate from another type non-aqueous sol–gel solution [35]. Second, stress very near the SUS304 substrate might have been rather compressive, as will be described in Section 4.1.2, making the crack initiation from sites near the substrate unfeasible. Excessive compression can cause wedging or buckling [29,36] as well as void collapse, but these phenomena were not observed in the present studies.

In the early stages of high-temperature annealing, the formation of vertical cracks must inevitably have enhanced the local dissipation of humidity and organics. In some instances, the local penetration of O from the environment might have been enhanced, promoting oxidation of remaining organics. These situations, together with the effect of tensile stress, should have promoted the further propagation of the cracks.

However, the fact that many of the observed cracks did not penetrate the sample interlayers indicated that adherence between the silica coating and the substrate was sufficient, and adherence could have provided an additional boundary condition for crack formation and exfoliation as described in Section 4.1.2.

Some definite initiation or triggering points, such as inclusion particles, could be observed in the OM images, and some of the shallow cracks were associated with ridges, though apparent triggering points were not observed for many of the shallow cracks. These cracks might have been initiated by nanoscale features not observed in the present microscopy images. Furthermore, the cracks appear to have propagated laterally in early stages before progressing to vertical propagation, as depicted schematically in Fig. 9(i), rather than propagating in the opposite order of directions (Fig. 9(ii)). This proposed lateral propagation mechanism is supported by OM data: many long, shallow cracks were observed, whereas deep, laterally short cracks were rarely observed. Two examples of such shallow cracks are visible in the top right portion of

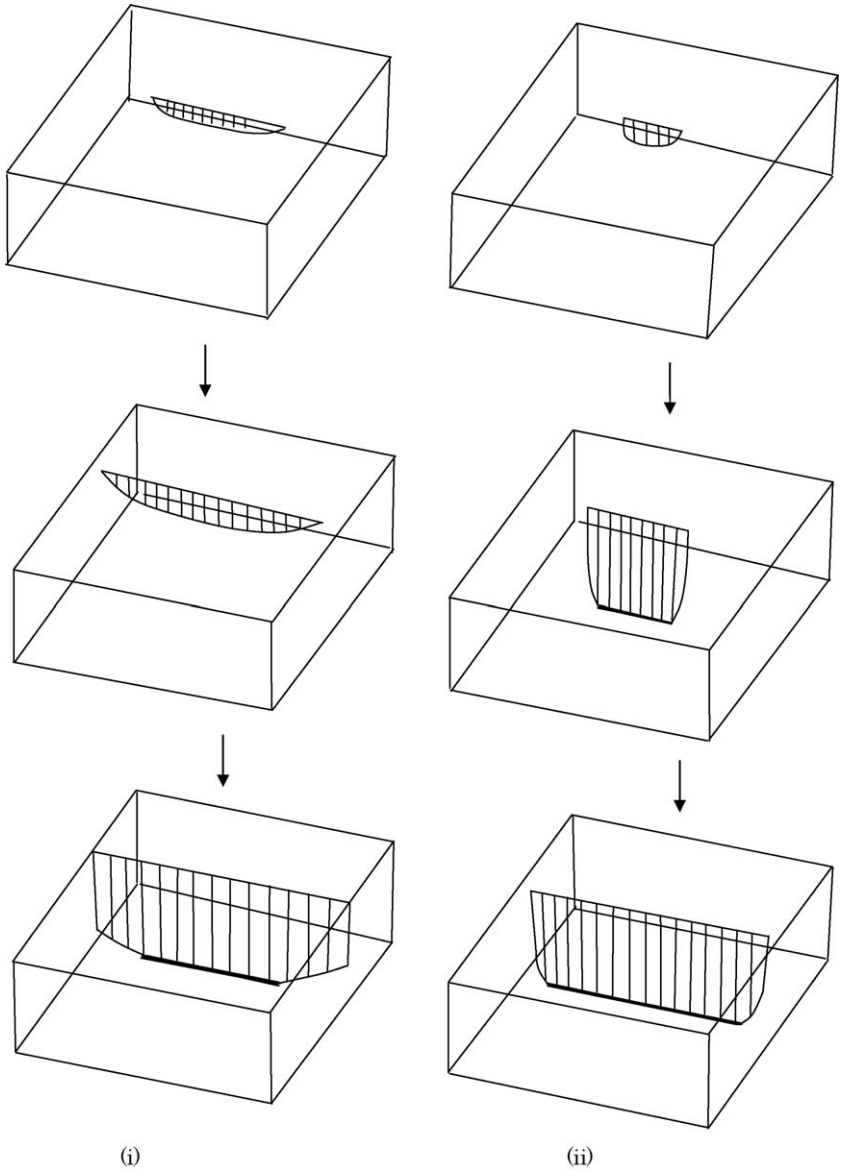

Fig. 9. Two possible modes of crack propagation in the silica coatings: (i) longitudinal propagation and (ii) depth propagation.

Fig. 4(ii), but there are also many shallow and laterally long ones that are not shown here.

4.1.2. Termination and diversion of vertical cracks

As mentioned above, vertical cracks sometimes approached the SUS304 surface but were often terminated before reaching the surface. Two major termination mechanisms are plausible: the tensile stress might have been smaller at greater depths within the silica coating (see also Section 4.1.1), or the silica matrix might have increased in rigidity during annealing. (The matrix also might have increased in toughness against vertical fracturing, as described in Part II, Section 4.3.)

As shallow cracks propagated downward and became deep cracks, some approached the SUS304 substrate. However, some of these cracks were instead diverted upon approaching the substrate, propagating laterally along the edge of the outermost interlayer, as seen in Fig. 8, rather than contacting the substrate. Although the case shown in Fig. 8, in which a vertical crack appears to have propagated to SUS along an inclusion particle (which must have dropped off before TEM observations), seems to be a rather special case, a more regular-type top-down propagation of a deep vertical crack in absence of a directly guiding particle most likely took place in the contacting vicinity of this point. Most likely, the majority of the vertical cracks were unable to penetrate the interlayers of the sample because properties of the interlayers, especially of the innermost one, must have prevented such penetration, as described just below.

A strongly reducing environment due to the presence of metallic Cr (and Si) in SUS is expected to be found at the surface of the substrate. Assuming that all of the O atoms present in the innermost interlayer were bonded to Cr, a Cr valence $\geq$3+ would result in an oxygen deficiency (*i.e.* $39.1 \times 3/2 = 58.7 > 44.9$ for location 'D' in Table 2); therefore, the valence of Cr was assumed to be $<$3 in the innermost interlayer. Since an abundance of Cr^{2+} has been reported sometimes in CrO_x [37] and since inorganic Cr^{+} is usually an unstable species (*i.e.* such reports are rare), the Cr in the innermost interlayer might have been mostly Cr^{2+}. As for Si, a valence of less than 4+ is strongly suggested from the XPS results shown in Part II, in spite of the slight ambiguity in the interpretation of the XPS spectra [38]. Nevertheless, the same spectra also indicate that the O-deficient layer clearly could not have been the major constituent of the entire coating. The adherent nature of SiO_x [39] and CrO_x [40] is believed to have promoted tenacious bonding between the coating film and the SUS304 substrate, thus preventing the penetration of vertical cracks through the innermost interlayer. Additionally, expected compressive stress in the innermost interlayer might have prevented the penetration of vertical cracks. The formation of this interlayer is compressive in that it consists of a volume-swelling reaction involving the oxidation of metallic elements in SUS304. Such compressive stress is expected to hinder crack propagation as well as initiation [41,42], unless the stress is extensive enough to induce large defects, *e.g.* wedging [29], buckling [36] and spallation [43]; which were not observed in the present samples. Neither the voids in the underlying SUS304 seem to have collapsed (typically in Fig. 7, and see also Section 4.2.3). Then it follows that the stress in the interlayers must have been moderately compressive. I believe moderately oxidizing conditions present at the silica/SUS interface during annealing caused this moderate strength of compression.

Notably, for the present study it was also assumed that free electrons and mobile positive holes were not abundant in the silica coating, because such highly conductive inorganic Cr–Fe–Si–Ni sub-oxides are scarcely reported. However, when trying to interpret such a distinct O-deficiency within the innermost interlayer, interesting results were obtained. Specifically, if the oxidation states of Fe, Cr, and O were assumed to be Fe^{2+}, Cr^{2+}, and O^{2-}, respectively, the calculated amount of O was insufficient (*i.e.* $10.2 + 39.1 = 49.3 > 44.9$ for location 'D' in Table 2) even when the presence of Si and Ni was neglected. Further investigation of the mechanical, physical, and chemical properties of Cr–Fe–Si–Ni sub-oxides is necessary. In particular, other reports [44] suggest both the difficulty and importance of controlling the properties of O-deficient sub-oxides such as those observed in the present study. Other reports [45,46] have suggested the possibility of Ni^{+} and Fe^{+} formation in quite special inorganic conditions, but their presence seem to be ambiguous.

At any rate, the specifically natured innermost interlayer of the present samples most likely consisted largely of highly O-deficient sub-oxides such as CrO_x and SiO_x and contributed largely to adherence.

4.1.3. Exfoliation

Deep vertical cracks terminated either without approaching the interlayers or after changing direction by propagating laterally along the outer edge of the interlayers. In cases in which a lateral crack propagated a long distance, the silica film should have been eventually exfoliated, but such exfoliation occurred in only a few exceptional cases within the present samples. The adherence of the silica film to the substrate seemed to have been largely excellent owing to the mechanisms described in Section 4.1.2. Additionally, graded element distributions near the interlayers also might have prevented exfoliation of the silica coating. These mechanisms of adherence are quite different from those previously reported for Si–C-containing soft sol–gel silica coatings on SUS [23].

Furthermore, the geometric constraints within the sample also might have influenced the silica film's tendency to exfoliate. That is to say, as illustrated schematically in Fig. 10, an area of silica coating surrounded by deep vertical cracks at short distances from each other might have tended to exfoliate, by some reason, more readily than that surrounded by long, distant deep vertical cracks. This proposed tendency is somewhat supported by Figs. 4 and 6. In Fig. 4, a flaky exfoliated film was observed on the small purple area. I think the coatings' tendency to curl upward may be at least due to the larger escaping rates of organics and humidity near both the outermost surface and a deep vertical crack than on the outermost surface far from deep cracks.

As high-temperature annealing proceeded, the almost non-porous silica matrix might have increased in rigidity without

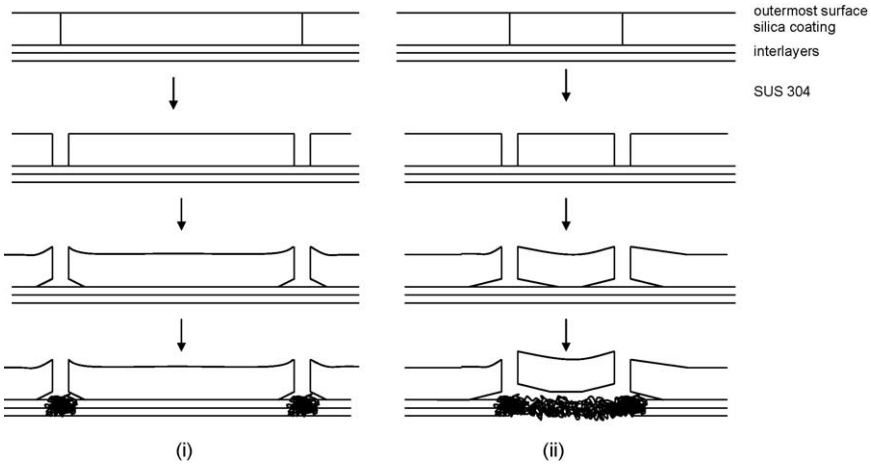

Fig. 10. Schematic models of exfoliation of a silica coating in areas surrounded by deep cracks separated from each other by (i) long distances and (ii) short distances. Interlayers are exaggerated in each drawing.

becoming appreciably brittle (see Part II). During this time, the adherence of the coating likely remained persistent as described above, and the diffusivity of O in silica matrix likely decreased (see also Part II). In such a case, lateral cracks as well as vertical cracks would be terminated, thus hindering massive exfoliation.

4.2. Ridges

The formation of ridges within the sample is undesirable since such ridges tend to promote additional sample irregularities. In the interest of optimizing synthetic strategies so as to eliminate such ridges, the mechanisms of ridge evolution are discussed below.

4.2.1. Overall mechanisms of ridge evolution and termination

Ridge development must have stopped during the long term ~500 °C annealing process, because of the TEM image (Fig. 7(iv)) showing that the outer part of the ridge is almost separated from the SUS304 substrate by the next innermost interlayer, indicating that the diffusion of metallic elements from SUS304 into the ridge stopped after some duration of annealing. Fig. 7 also indicates that some grain boundaries of SUS304 were accompanied by ridges, although others were not.

I believe that the ridges might have evolved and terminated as follows: the presence of nanoscale defects within the innermost interlayer might have promoted the diffusion of metallic elements from the SUS304 to the silica coating. These defects are described in more detail in Section 4.2.2. Before the later stage of 500 °C annealing, metallic elements (Fe, Cr, and Ni) might have been slightly oxidized, incorporated in silica, and diffused at various rates, with Fe and Ni diffusing more quickly than Cr. This diffusion would have left atomic-scale vacancies in the SUS304; the vacancies then might have coagulated sometimes at sink sites (*e.g.* grain boundaries) of SUS and formed voids as shown in Fig. 7(ii) and (iv). In silica, Fe, Ni, and Cr were further (but mildly) oxidized by reaction with O or O-containing species already present in the coating or diffused inward from the outermost surface. After some time, further extension of ridge growth stopped, with the termination mechanisms described in Section 4.2.3.

The tensile stress inside and around the ridges might have been relaxed to some extent by the volume-swelling oxidation of metallic elements (mostly that of Fe). Overall, the area inside the ridges was rather O-deficient, as determined by EDX analysis (Table 2).

4.2.2. Nanoscale defects in the innermost interlayer triggering ridges

The OM results showed that most of the ridges were web-like, as if following the course of grain boundaries present in the SUS304 substrate, and these grain boundaries are observed in the TEM images in Figs. 7(i), (ii), and (iv). I believe that, although sensitization of SUS304 is feared to become severe above ~600 °C [49], some change (most probably accumulation or depletion of elements, see just below) occurred at SUS304 grain boundaries as low as ~500 °C, and brought about nanoscale defects at the innermost interlayer, thus promoting the diffusion of metallic elements from SUS into silica coating and subsequent formation of ridges. The outward diffusion of metallic elements from deeper parts of SUS through grain boundaries might have been activated to some extent by atomic vacancies injected into the SUS304 through the defect sites [47]. These atomic vacancies might also have coagulated to bare voids. Phenomena at SUS304 grain boundaries are complicated and depend greatly on temperature in the range of ~450 to ~850 °C [48]. Sensitization is usually ascribed to the accumulation of Cr-carbide [48], B [10], or both [49] at the grain boundaries. Other elements, such as N [50], O [51], P [49], Mo [49] and H [52] exist as minor elements in SUS and could have interacted with SUS grain boundaries.

From OM observations, some streak-like ridges seem to have formed at places where scratches were already present on the as-received SUS304 substrates. This observation indicates that some of the defects of the innermost interlayer were triggered by scratches on the SUS304. Inclusion particles of MnS have been reported to appear on SUS304 surfaces but

probably were not the major triggers at least in the present case, because such particles are usually several μm in diameter [53], but such large ridges were not observed in the present case.

Similarly shaped but much bigger ridges have been observed for silica coatings on a low-C AISI316L interface [8]. I speculate that defects other than those related to the carbides at the SUS grain boundaries might have triggered the formation of such ridges.

4.2.3. Termination of ridge growth

Ridge growth seems to have stopped after some duration of annealing, meaning that some termination mechanism must have occurred. That process may have been associated with the collapse of the aforementioned nanoscale defects in the innermost interlayer. Additionally, the second innermost interlayer, which was diffuse and Cr-rich, might have gradually covered the nanoscale defects. These two healing mechanisms might have resulted from the volume-swelling oxidation reaction described in Section 4.1.2. Another possible termination mechanism is that voids formed in the SUS304 substrate could have blocked the further diffusion of metallic elements from SUS304. Furthermore, inert Ni might have accumulated in SUS near the defect sites during ridge growth, because the diffusivity of Ni in SUS304 is thought to be small [54]. Finally, the diffusion of O, Fe, Cr, and Ni in the silica coating probably decreased during the ∼500 °C annealing process; this supposition is supported by the almost fixed gradients of Fe, Cr, and Ni distribution as well as of oxygen deficiency observed by TEM/EDX around the interlayers and ridges after 500 °C annealing. These gradients indicate that diffusion of Fe, Cr, Ni, and O became slow enough to stifle the oxidation of SUS at least in the later stage of 500 °C annealing. Still other mechanisms, *e.g.* so-called 'desensitization' of SUS304 [48], could have occurred and contributed to the termination of ridges.

4.2.4. Cracks guided by ridges

As shown in Figs. 3 and 5, both shallow and deep vertical cracks propagated along a ridge sometimes. I speculate that the mechanisms for this type of crack initiation, propagation, and termination are those illustrated schematically in Fig. 11. Because ridge formation is a volume-swelling oxidation reaction, it could have relaxed the tension around the ridges. This relaxation then could have allowed tension (see Part II) to be concentrated to some extent near the outermost surface, evoking initiation of the cracks. Notably, the downward propagation of cracks was to some extent hindered (or diverted) by the stress relaxation around the ridges themselves. Although Fig. 7(ii) also supports such speculations, the phenomena governing such ridge-guided crack formation are likely complicated since so many related factors are involved (*e.g.* types of grain boundaries in the underlying SUS304 substrate).

4.3. Remarkable inertness of metallic Ni toward oxidation

Only very small amounts of Ni were incorporated into the silica matrix in the present studies, with the exception of the innermost interlayer and ridges, as evidenced by EDX analysis. These observations agreed with the general inertness of metallic Ni toward oxidation [55] and the reported enhancement of its inertness when in contact with silica [56]. I believe that this synergistic effect occurred because Ni is generally immiscible with silica [57] and SiO_x [58]. (However, an appreciable amount of Ni can be incorporated under special reducing conditions [59], and careful additional study is required.) Additionally, SiO_x films are generally good diffusion barriers for gases [60] and metallic elements [61].

Interestingly, the Ni content was small in the second interlayer, which was rich in Cr and poor in Si. Generally, Ni is fairly soluble in SiO_2–Cr_2O_3 systems [62]. The reason for the low Ni content in the second interlayer is not clear, but presumably the high Cr concentration displaced some of the Ni or prevented its diffusion.

To summarize, the inertness of metallic Ni toward oxidation seems to be promoted by the coexistence of Si and Cr both in appropriate (but delicate) amounts and states, under the moderate oxidation conditions of the present study.

4.4. Effects of other minor elements in SUS304

Mn [63], Cu [63], and Co [64] are sometimes present in small quantities in SUS304. However, they seem not to have greatly influenced the observed properties of the present silica coatings with interlayers and ridges, because these elements tend to be incorporated into silica matrices in very low concentrations (*i.e.* diluted). In fact, Mn and Co were not detected by EDX in the present studies. Cu was detected, but the presence of Cu can likely be attributed to the Cu content of the TEM support grid, and therefore was not included in Table 2. Furthermore, strong interactions between these three elements and the grain boundaries of stainless steels such as SUS304 are rarely reported. Nevertheless, some additional investigation is needed on the possible effects of these elements themselves and compounds containing these elements, such as MnS particles [53].

Interestingly, examples in the literature strongly suggest that the presence of moderate amounts of N enhances the adherence of oxide films on stainless steels, even after most of this N has been eliminated from the sample [65]. Although N content in the SUS substrate was minor, this non-negligible amount could have come from the bulk, because N can diffuse rapidly in SUS304 at ∼500 °C [9], and most probably much more rapidly along SUS grain boundaries. Sometimes N behaves uniquely in sub-oxides [66], and the seemingly unusual behavior of N near metal/ceramic junctions has been reported as well [67]. In the present study, N presumably did not negatively affect the quality of the silica films. Also, it is possible that N in the present samples interacted with the SUS304 grain boundaries, as described in Section 4.2.

Typically, B is present in only very small quantities in SUS304, so the present samples were not analyzed for B content. However, further studies must be undertaken to investigate the complicated effects of S [68], P [49], Mo [49],

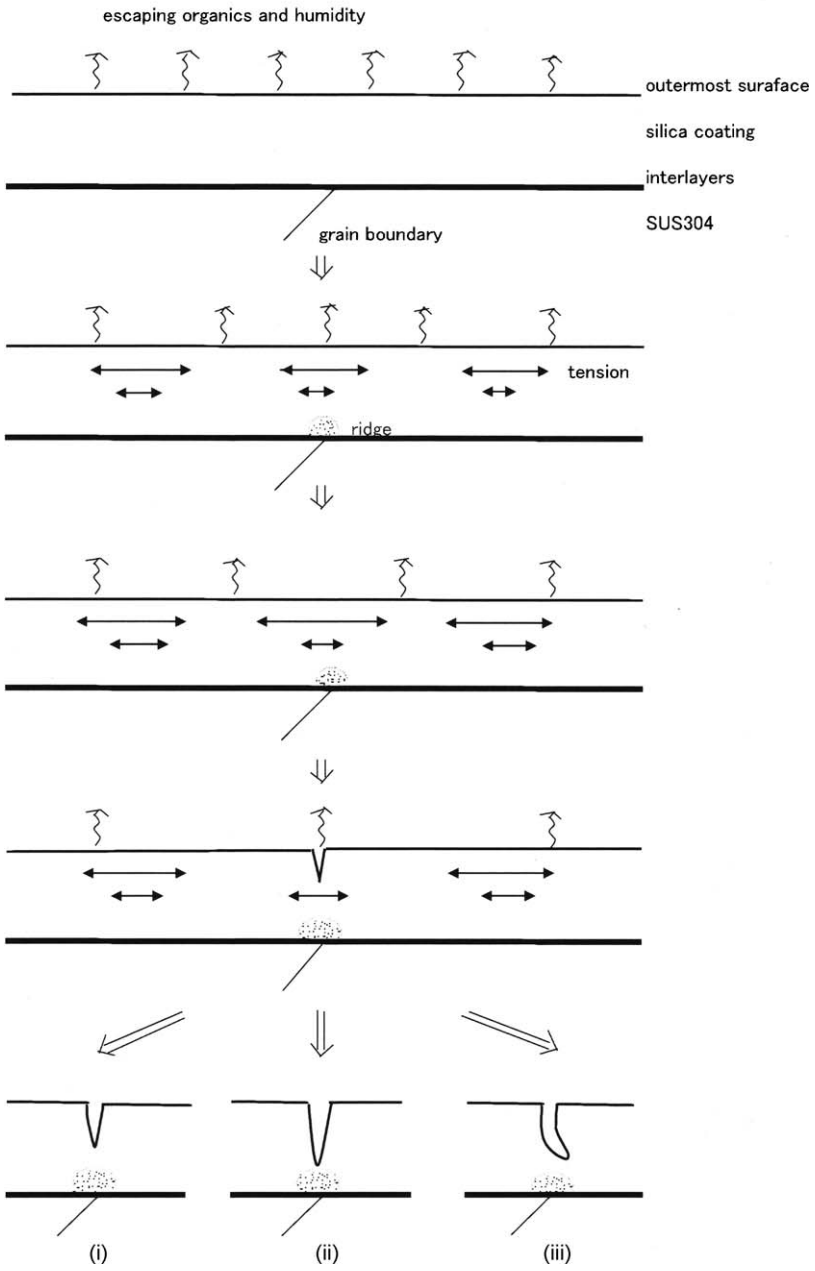

Fig. 11. Schematic model of crack evolution along a ridge in a silica coating. (i) Crack terminated without reaching a ridge, (ii) crack reaching a ridge, and (iii) crack diverted. In each drawing, the interlayers are gathered in a thick solid line.

and B [10], especially in relation to the SUS304 grain boundaries and the interlayers.

4.5. Practical problems in the near future

Silica coating so-formed on SUS304 was not with 'poor quality' but unfortunately not with 'sufficiently good quality'. Also some additional problems are likely to arise in practical applications. Not only the exfoliated parts but also the ridges left in the deeper part of the coating, the voids left in the adjacent SUS304 substrate, and the deactivated shallow cracks left near the outer surface might flare up again as defect points that promote degradation under more prolonged or severe conditions of use. The long-term stability of this coating is doubtful even when used under room temperature conditions, because much humidity seems to have been incorporated into the silica matrix after cooling (see also Part II, especially Section 4.3). To overcome these problems, suggestions to improve silica coating is presented in Part II, Section 4.5.

5. Conclusions

Silica films were formed on SUS304 by means of a previously studied non-aqueous sol–gel method. The coated specimens were annealed at 500 °C and analyzed by a variety of microscopic techniques, yielding the following conclusions:

(1) The thicknesses of the silica films ranged from ∼350 to ∼1000 nm. The films were largely uniform, compact, and adherent, with few organics remaining in the films after the annealing process.
(2) However, the films contained both shallow and deep cracks as well as exfoliated sites. Most of the cracks were initiated near the outermost surface of the silica coating and propagated first laterally, then vertically toward the SUS304 substrate. In some cases the cracks were rather shallow, terminating without approaching the SUS304. The lateral propagations of the deep cracks were basically independent of the occurrence of ridges or pre-existing scratches in the SUS304 substrate. But there were some shallow cracks running along ridges that had evolved in the silica coating. The cause of these cracks is discussed in more detail in Part II of this report.
(3) Three consecutive interlayers were formed during the annealing process. The innermost interlayer was ∼5 nm thick and formed a tenacious bonding between SUS304 and silica. The other two interlayers were rather diffuse. These interlayers were all O-deficient, but the O deficiency was most marked for the innermost interlayer. The innermost interlayer contained metallic elements with EDX intensities that decreased in the order Cr > Fe ≫ Si > Ni, and the valence of Cr in this layer seems to be mostly 2+. The second innermost interlayer exhibited EDX intensities that decreased in the order Cr ≫ Si ≫ Fe ≫ Ni, and the outermost interlayer exhibited EDX intensities that decreased in the order Si > Fe ≫ Cr (Ni was not detected in this interlayer). Ni, Cr, Si, and sometimes Fe (each with various valence states) probably acted cooperatively to provide relatively good conditions, especially adherence, for the coating.
(4) Many ridges formed in the silica coating near its interface with the SUS304 substrate. Most of these ridges were close to SUS grain boundaries. In some cases, voids were present in the adjacent SUS304. However, many grain boundaries existed without ridges being located nearby. Additionally, some ridges formed near scratches already present on SUS304. These ridges most likely resulted from the diffusion of metallic elements into the silica matrix through nanoscale defects in the innermost interlayer. The areas inside the ridges were somewhat O-deficient and exhibited metallic element EDX intensities that decreased in the order Fe > Si ≫ Ni ≒ Cr. Ridge development seemed to be stifled at some point during the annealing process.

Part II of this report will further investigate the mechanical and spectroscopic characterization of these coatings, and also provide insight into interlayer and crack formation characteristics and mechanisms. Suggestions for creation of 'good-quality' silica coatings will be presented on the basis of results obtained in Parts I and II.

Acknowledgements

I gratefully acknowledge the useful discussions with and cooperation of researchers and staff of the AIST (National Institute of Advanced Industrial Science and Technology), Kobe Steel, Kobelco Kaken Co., Ltd., NSG Techno-Research Co., Ltd., Keyence Co., Ltd. and Collet Kogyo Co., Ltd.

References

[1] S. Ono, Y. Nishi, Chromium-free corrosion resistance of metals by ceramic coating, J. Am. Ceram. Soc. 84 (12) (2001) 3054–3056.
[2] D.C.L. Vasconcelos, J.A.N. Carvalho, M. Mantel, W.L. Vasconcelos, Corrosion resistance of stainless steel coated with sol–gel silica, J. Non-Cryst. Solid 273 (1–3) (2000) 135–139.
[3] O. de Sanctis, L. Gómez, N. Pellegri, C. Parodi, A. Marajofsky, A. Durán, Protective glass coatings on metallic substrates, J. Non-Cryst. Solid 121 (1–3) (1990) 338–343.
[4] M.J. Bennett, M.R. Houlton, R.W.M. Hawes, The improvement by a CVD silica coating of the oxidation behaviour of a 20% Cr/25% Ni niobium stabilized stainless steel in carbon dioxide, Corr. Sci. 22 (2) (1982) 111–133.
[5] S. Ono, H. Tsuge, Y. Nishi, S.-i. Hirano, Improvement of corrosion resistance of metals by an environmentally friendly silica coating method, J. Sol–Gel Sci. Technol 29 (3) (2004) 147–153.
[6] J.-S. Chang, Next generation integrated electrostatic gas cleaning systems, J. Electrostat. 57 (3–4) (2003) 273–291.
[7] G.A. Garzino-Demo, F.L. Lama, Friction and wear of uncoated or SiO_2-coated 329 stainless steel and of uncoated or AlN-coated aluminium surfaces, Surf. Coat. Technol. 68/69 (1994) 507–511.
[8] W. Hänni, H.E. Hintermann, D. Morel, A. Simmen, Silica coatings on strongly passivated substrates, Surf. Coat. Technol. 36 (1–3) (1988) 463–470.
[9] O. de Sanctis, L. Gómez, N. Pellegri, A. Durán, Behaviour in hot ammonia atmosphere of SiO_2-coated stainless steels produced by a sol–gel procedure, Surf. Coat. Technol. 70 (2–3) (1995) 251–255.
[10] M. Kurban, U. Erb, K.T. Aust, A grain boundary characterization study of boron segregation and carbide precipitation in alloy 304 austenitic stainless steel, Scripta Mater. 54 (6) (2006) 1053–1058.
[11] S. Benayoun, L. Fouilland-Paillé, J.J. Hantzpergue, Microscratch test studies of thin silica films on stainless steel substrates, Thin Solid Films 352 (1–2) (1999) 156–166.
[12] J. Pou, P. González, E. Galcía, D. Fernández, J. Serra, B. León, S.R.J. Saunders, M. Pérez-Amor, High-temperature corrosion-resistant ceramic coatings obtained by laser chemical vapour deposition, Vacuum 45 (10–11) (1994) 1035–1037.
[13] M. Nakayama, J. Yano, K. Nakaoka, K. Ogura, Electrodeposition of composite films consisting of polypyrrole and mesoporous silica, Synth. Met. 128 (1) (2002) 57–62.
[14] Y. Castro, B. Ferrari, R. Moreno, A. Durán, Coatings produced by electrophoretic deposition from nano-particulate silica sol–gel suspensions, Surf. Coat. Technol. 182 (2–3) (2004) 199–203.
[15] Y. Castro, B. Ferrari, R. Moreno, A. Durán, Corrosion behaviour of silica hybrid coatings produced from basic catalysed particulate sols by dipping and EPD, Surf. Coat. Technol. 191 (2–3) (2005) 228–235.
[16] S. Nitta, Y. Kimura, Formation of SiO_2 thin film on SUS304 stainless steel by liquid phase deposition, J. Soc. Mater. Sci. Jpn. 43 (494) (1994) 1437–1443 (in Japanese).
[17] F. Bauer, U. Decker, A. Dierdorf, H. Ernst, R. Heller, H. Liebe, R. Mehnert, Preparation of moisture curable polysilazane coatings. Part I. Elucidation of low temperature curing kinetics by FT-IR spectroscopy, Prog. Org. Coat. 53 (3) (2005) 183–190.
[18] G. Della Giustina, G. Brusatin, M. Guglielmi, F. Romanato, Direct nanopattern of hybrid sol–gel films, Mater. Sci. Eng. C 27 (5–8) (2007) 1382–1385.
[19] C.J. Brinker, G.W. Scherer, Sol–Gel Science, Academic Press, San Diego, 1990 (Chapter 13).
[20] M. Guglielmi, D. Festa, P.C. Innocenzi, P. Colombo, M. Gobbin, Borosilicate coatings on mild steel, J. Non-Cryst. Solid 147 (148) (1992) 474–477.

[21] A.R. Di Giampaolo Conde, M. Puerta, H. Ruiz, J. Lira Olivares, Thick aluminosilicate coatings on carbon steel via sol–gel, J. Non-Cryst. Solid 147 (148) (1992) 467–473.
[22] J.V. Littlejohns, A.J. Daugulis, Oxygen transfer in a gas–liquid system containing solids of varying oxygen affinity, Chem. Eng. J. 129 (1–3) (2007) 67–74.
[23] K. Izumi, H. Tanaka, Y. Uchida, N. Tohge, T. Minami, Influence of firing conditions on adhesion of methyltrialkoxysilane-derived coatings on steel sheets, J. Non-Cryst. Solid 147–148 (1992) 483–487.
[24] P. Innocenzi, M.O. Abdirashid, M. Guglielmi, Structure and properties of sol–gel coatings from methyltriethoxysilane and tetraethoxysilane, J. Sol–Gel Sci. Technol. 3 (1994) 47–55.
[25] T. Maeseto, T. Kitaoka, S. Toriu, S. Fujii, M. Kobune, Cause of exfoliation of glass lining layer on stainless steel, Kagaku Kogaku Ronbunshu 27 (6) (2001) 761–764 (in Japanese).
[26] M. Takemori, Low temperature synthesis of a silica-based glass-like adherent film by a sol–gel method, J. Mater. Sci. Lett. 20 (2001) 151–154.
[27] A. Boelle, J.A. Roger, B. Canut, J. Mugnier, M. Pitaval, Sol–gel low-temperature preparation of silica films: RBS, TEM and MOS C-V characterization, Appl. Surf. Sci. 46 (1–4) (1990) 200–205.
[28] U. Bräutigam, H. Bürger, W. Vogel, Some aspects of property tailoring of sol–gel derived thin SiO_2 films, J. Non-Cryst. Solid 110 (2–3) (1989) 163–169.
[29] K.S. Chan, A mechanics-based approach to cyclic oxidation, Metall. Mater. Trans. A 28 (1997) 411–422.
[30] J. Liu, J.M. O'Reilly, T.W. Smith, P.N. Prasad, Photopatterning hybrid sol–gel glass materials prepared from ethylene tellurate and alkoxysilane, J. Non-Cryst. Solid 351 (30–32) (2005) 2440–2445.
[31] H. Schmidt, Inorganic-organic composites by sol–gel techniques, J. Sol–Gel Sci. Technol. 1 (1994) 217–231.
[32] M.S. Gruszkiewicz, J. Horita, J.M. Simonson, R.E. Mesmer, J.B. Hulen, Water adsorption at high temperature on core samples from The Geysers geothermal field, California, USA, Geothermics 30 (2–3) (2001) 269–302.
[33] C.J. Brinker, G.W. Scherer, Sol–Gel Science, Academic Press, San Diego, 1990 (Chapters 5–8).
[34] H. Ryu, D. Suh, M.C. Peak, Fabrication of nanoimprinted curved feature for focusing grating coupler using hydrogen silsesquioxane mold., Curr. Appl. Phys. 6S1 (2006) e121–e124.
[35] Japan Patent L2003009732.
[36] A. Bousquet, V. Bursikova, A. Goullet, A. Djouadi, L. Zajickova, A. Granier, Comparison of structure and mechanical properties of SiO_2-like films deposited in O_2/HMDSO pulsed and continuous plasmas, Surf. Coat. Technol. 200 (22–23) (2006) 6517–6521.
[37] B. Liu, P. Šindelář, Y. Fang, K. Hasebe, M. Terano, Correlation of oxidation states of surface chromium species with ethylene polymerization activity for Phillips CrO_x/SiO_2 catalysts modified by Al-alkyl cocatalyst, J. Mol. Catal. A: Chem. 283 (1–2) (2005) 142–150.
[38] J. Serra, P. González, S. Liste, C. Serra, S. Chiussi, B. León, M. Pérez-Amor, H.O. Ylänen, M. Hupa, FTIR and XPS studies of bioactive silica based glasses, J. Non-Cryst. Solid 332 (1–3) (2003) 20–27.
[39] J.H. Lee, D.S. Kim, Y.H. Lee, B. Farouk, Mechanical properties of a-C:H and a-C:H/SiO_x nanocomposite thin films prepared by ion-assisted plasma-enhanced chemical vapor deposition, Thin Solid Films 280 (1–2) (1996) 204–210.
[40] S. Lopez-Esteban, E. Saiz, S. Fujino, T. Oku, K. Suganuma, A.P. Tomsia, Bioactive glass coatings for orthopedic metallic implants, J. Eur. Ceram. Soc. 23 (15) (2003) 2921–2930.
[41] A.J. Blattner, R. Lakshminarayanan, D.K. Shetty, Toughening of layered ceramic composites with residual surface compression: effects of layer thickness, Eng. Fract. Mech. 68 (1) (2001) 1–7.
[42] M. Pavese, P. Fino, A. Ortona, C. Badini, Potential of SiC multilayer ceramics for high temperature applications in oxidising environment, Ceram. Int. 34 (1) (2008) 197–203.
[43] S. Baleix, G. Bernhart, P. Lours, Oxidation and oxide spallation of heat resistant cast steels for superplastic forming dies, Mater. Sci. Eng. A 327 (2) (2002) 155–166.
[44] L.K. Thomas, W. Pekruhn, T. Chunhe, A. Schröder, Properties of solar selective absorbing Cr–SiO cermets after high temperature treatment, Solar Energy Mater. 16 (1–3) (1987) 133–141.
[45] W. Low, J.T. Suss, Jahn-teller effect of Ni^{1+} and Cu^{2+} in single crystals of calcium oxide, Phys. Lett. 7 (5) (1963) 310–312.
[46] A.K. Garrison, Electron paramagnetic resonance of NaF Fe^{+}, Mater. Res. Bull. 2 (2) (1967) 155–164.
[47] J. Dryzek, C. Wesseling, E. Dryzek, B. Cleff, Migration of vacancies in stainless steel measured by positron annihilation, Mater. Lett. 21 (2) (1994) 209–214.
[48] A. Yae Kina, V.M. Souza, S.S.M. Tavares, J.M. Pardal, J.A. Souza, Microstructure and intergranular corrosion resistance evaluation of AISI 304 steel for high temperature service, Mater. Charact. 59 (5) (2008) 651–655.
[49] S.R. Ortner, A stem study of the effect of precipitation on grain boundary chemistry in AISI 304 steel, Acta Metall. Mater. 39 (3) (1991) 341–350.
[50] Z.Z. Yuan, Q.X. Dai, X.N. Cheng, K.M. Chen, Microstructural thermostability of high nitrogen austenitic stainless steel, Mater. Charact. 58 (1) (2007) 87–91.
[51] I. Sato, M. Takaki, T. Arima, H. Furuya, K. Idemitsu, Y. Inagaki, M. Momoda, T. Namekawa, Oxidation behavior of modified SUS316 (PNC316) stainless steel under low oxygen partial pressure, J. Nucl. Mater. 304 (1) (2002) 21–28.
[52] Q. Yang, J.L. Luo, Martensite transformation and surface cracking of hydrogen charged and outgassed type 304 stainless steel, Mater. Sci. Eng. A 288 (1) (2000) 75–83.
[53] P. Schmuki, H. Hildebrand, A. Friedrich, S. Virtanen, The composition of the boundary region of MnS inclusions in stainless steel and its relevance in triggering pitting corrosion, Corr. Sci. 47 (5) (2005) 1239–1250.
[54] E.P. Simonen, L.A. Charlot, S.M. Bruemmer, Quantification of defect-solute coupling from inverse-Kirkendall segregation, J. Nucl. Mater. 225 (1995) 117–122.
[55] W. Brückner, S. Baunack, M. Hecker, J. Thomas, S. Groudeva-Zotova, C.M. Schneider, Oxidation of NiFe (20 wt.%) thin films, Mater. Sci. Eng. B 86 (3) (2001) 272–275.
[56] L. Narváez, O. Dominguéz, J.R. Martínez, F. Ruiz, Preparation of (Ni-B)/SiO_2, Ni/SiO_2 and NiO/SiO_2 nanocomposites, J. Non-Cryst. Solid 318 (1–2) (2003) 37–42.
[57] B. Canut, A. Merlen, V. Teodorescu, C. Ghica, C.S. Sandu, S.M.M. Ramos, C. Bovier, R. Espiau de la Maestre, A. Broniatowski, H. Bernasr, Ion beam photography in sol–gel NiO–SiO_2 films, Nucl. Instr. Method. Phys. Res. B 209 (2003) 335–339.
[58] Y. He, J.Y. Feng, Q.L. Wu, A study of the correlation between nickel and the ultraviolet emission in SiO_x films, J. Crystal Growth 281 (2–4) (2005) 318–322.
[59] M. LIczka, K. Cholewa, Chromium, cobalt, nickel and copper as pigments of sol–gel glasses, J. Alloys Compd. 218 (1) (1995) 77–85.
[60] S. Iwamori, Y. Gotoh, K. Moorthi, Silicon oxide gas barrier films deposited by reactive sputtering, Surf. Coat. Technol. 166 (1) (2003) 24–30.
[61] T.J. Sarapatka, XPS and XAES study of interaction between Ni and Si(111), SiO_x/Si(111) supports, J. Electron Spectr. Rel. Phenom. 62 (4) (1993) 335–349.
[62] A. Duran, J.M. Fernandez Navarro, P. Mazon, A. Joglar, Coloured coatings containing mixed transition metal oxides, J. Non-Cryst. Solid 100 (1–3) (1988) 494–500.
[63] S. Sakka, S. Ito, K. Kamiya, Electronic spectra of transition metal ions in gel-derived and melt-derived glasses, J. Non-Cryst. Solid 71 (1–3) (1985) 311–315.
[64] F. Orgaz, H. Rawson, Characterization of various stages of the sol–gel process, J. Non-Cryst. Solid 82 (1–3) (1986) 57–68.
[65] C. Issartel, H. Buscail, E. Caudron, R. Cueff, F. Riffard, S. Perrier, P. Jacquet, M. Lambertin, Influence of nitridation on the oxidation of a 304 steel at 800 °C, Corr. Sci. 46 (9) (2004) 2191–2201.
[66] E.J. Friebele, D.L. Griscom, T.W. Hickmott, Nitrogen-associated paramagnetic defect centers in sputtered SiO_2 films, J. Non-Cryst. Solid 71 (1–3) (1985) 351–359.

[67] V. Leroux, J.C. Labbe, T.T. Nguyen, M.E.R. Shanahan, Wettability of non-reactive Cu/Si–Al–O–N systems. I. Experimental results, J. Eur. Ceram. Soc. 21 (6) (2001) 825–831.
[68] C.L. White, R.A. Padgett, R.W. Swindeman, Sulfur and phosphorus segregation to creep cavities and grain boundaries in 304 SS, Scripta Metall. 15 (7) (1981) 777–782.

Makoto Takemori received the Ph.D degree from Institute of Industrial Science, the University of Tokyo, in March 1984. The author was a special research student during April 1984–March 1985 at the Japan Atomic Energy Research Institute and is currently researcher at AIST since April 1985.